Analysis of Recent Anthropogenic Surface Emissions from Bottom-up Inventories and Top-down Estimates: Are Future Emission Scenarios Valid for the Recent Past?

N. Elguindi[1], C. Granier[1,2], T. Stavrakou[3], S. Darras[4], M. Bauwens[3], H. Cao[5], C. Chen[6,7], H.A.C. Denier van der Gon[8], O. Dubovik[6,7], T.M. Fu[9], D. Henze[10], Z. Jiang[11], J.J.P. Kuenen[8], J. Kurokawa[12], C. Liousse[1], K. Miyazaki[13], J.-F. Müller[3], Z. Qu[10,14], K. Sekou[15,16], F. Solmon[1], B. Zheng[17]

[1]Laboratoire d'Aérologie, CNRS, Université de Toulouse, France
[2]NOAA/ESRL/CSD- CIRES/University of Colorado, Boulder, CO, USA
[3]Royal Belgian Institute for Space Aeronomy, Brussels, Belgium
[4]Observatoire Midi-Pyrénées, Toulouse, France
[5]University of Colorado Boulder, USA
[6]Laboratoire d'Optique Atmosphérique (LOA), UMR8518 CNRS, Université de Lille, Villeneuve D'ASCQ, 59655, France
[7]GRASP-SAS, Remote Sensing Developments, Université de Lille, Villeneuve D'ASCQ, 59655, France
[8]TNO, dept. Climate, Air and Sustainability, Utrecht, The Netherlands
[9]School of Environmental Science and Engineering, Southern University of Science and Technology, Shenzhen, Guangdong Province, China
[10]Department of Mechanical Engineering, University of Colorado Boulder, Boulder, CO, USA
[11]School of Earth and Space Sciences, University of Science and Technology of China, Hefei, Anhui, 230026, China
[12]Asia Center for Air Pollution Research, 1182 Sowa, Nishi-ku, Niigata, Niigata, 950-2144, Japan
[13]Jet Propulsion Laboratory, California Institute of Technology
[14]John A. Paulson School of Engineering and Applied Science, Harvard University, Cambridge, MA, USA
[15]University PGC, UFR sciences Biologiques - Korhogo, Côte d'Ivoire
[16]Laboratoire de Physique de l'Atmosphère (LAPA-UFHB)
[17]Laboratoire des Sciences du Climat et de l'Environnement, CEA-CNRS-UVSQ, UMR8212, Gif-sur-Yvette, France

Corresponding author: N. Elguindi (elgn@aero.obs-mip.fr)

Key Points:

- Top-down emissions are generally within the range of bottom-up inventories and exhibit a similar level of uncertainty, or even less in regions such as China.
- In China, the U.S. and Europe emission trends in the last decade from SSP126 match most closely actual trends from bottom-up and top-down estimates.
- In Western Africa and India recent emission trends from low pollution control scenarios (SSP460 and SSP370, respectively) match most closely actual trends.

Abstract

This study compares recent CO, NO_x, NMVOC, SO_2, BC and OC anthropogenic emissions from several state-of-the-art top-down estimates to global and regional bottom-up inventories and projections from five SSPs in several regions. Results show that top-down emissions exhibit similar uncertainty as bottom-up inventories in most regions, and even less in some such as China. In general, for all species the largest discrepancies are found outside of regions such as the U.S., Europe and Japan where the most accurate and detailed information on emissions is available. In some regions such as China, which has undergone dynamical economic growth and changes in air quality regulations during the last several years, the top-down estimates better capture recent emission trends than global bottom-up inventories. These results show the potential of top-down estimates to complement bottom-up inventories and to aide in the development of emission scenarios, particularly in regions where global inventories lack the necessary up-to-date and accurate information regarding regional activity data and emission factors such as Africa and India. Areas of future work aimed at quantifying and reducing uncertainty are also highlighted. A regional comparison of recent CO and NO_x trends in the five SSPs indicate that SSP126, a strong-pollution control scenario, best represents the trends from the from top-down and regional bottom-up inventories in the U.S., Europe and China, while SSP460, a low-pollution control scenario, lies closest to actual trends in West Africa. This analysis can be a useful guide for air quality forecasting and near-future pollution control/mitigation policy studies.

1 Introduction

Anthropogenic activities such as energy production, industrial processes, transportation, agriculture and waste management are responsible for the emissions of gaseous and particulate pollutants which can both modify the climate and reduce air quality, leading to adverse impacts on the environment and human health. Accurate and up-to-date emission inventories are essential to understand the contribution of various human activities, model and predict the related changes in atmospheric composition, and design cost-effective mitigation strategies. Despite their paramount importance, large uncertainties and limitations exist in current state-of-the-art global and regional emission inventories (Crippa et al., 2018). Based on emission estimates from inventories, along with information regarding socio-economic, environmental, and technological

trends, future emission scenarios such as the Shared Socioeconomic Pathways (SSPs) are created and used by atmospheric and chemistry models to generate future climate and pollutant concentration projections. As such, uncertainties associated with current emission estimates are directly propagated into future scenarios of emission trajectories, model climate projections and air quality forecasts.

For a given chemical compound, emission inventories rely on the definition of key socio-economic sectors (i.e. road traffic) involving certain technologies (i.e. car engine) characterized by specific emission factors (i.e. CO emissions per unit of fuel used per km). This information is then scaled up using geographically distributed information of the corresponding activities (e.g. car traffic intensity map) to create large-scale gridded inventories. The complexity of emission modelling lies in the diversity of chemical species, as well as in the characterization and quantification of emission factors and sector activities, all of which are highly variable and influenced by socio-economic and environmental factors. Country-level indicators used to build global emission inventories and projections often lack up-to-date regional specific information, especially in developing regions. These inventories are largely created using emission factors (EF) that are representative of conditions in developed countries, such as Europe and North America. Although often an EF is selected that represents a low technology level, the origin of the EF data is from developed countries, thereby introducing large errors and uncertainties into the emission estimates for developing countries. Furthermore, the collection of data for all countries throughout the world takes considerable time; by the time the inventories are updated there is thus often a significant lag from the present day.

Alternatively, inverse modelling techniques, which constrain atmospheric models by observations to estimate surface emissions, have been used to derive emissions for various air pollutants (e.g. Miyazaki et al. 2017; Stavrakou et al. 2012; Müller et al. 2005; Arellano et al. 2004). A main advantage of these estimation techniques is their high spatial coverage, in particular when spaceborne atmospheric data are used as constraints. Another benefit is that they can provide more timely emission estimates than traditional bottom-up inventories, which are generally delayed by a few years. Inverse modelling has the potential to reduce uncertainty in air quality and chemistry climate models by providing more constrained emission data, especially in

106 regions of the world where bottom-up estimates are believed to be deficient. Nevertheless,
107 inverse modelling has its limitations and uncertainties that should be addressed and quantified.
108 Notably, uncertainties are associated with the use of atmospheric models, in particular their
109 representation of transport and chemical processes (e.g. Jiang et al., 2013; Stavrakou et al.,
110 2013). Another source of uncertainties is related to the observations used to constrain the models.
111 For example, satellite data intercomparison studies revealed large differences between different
112 retrievals of the same compound as well as significant biases against well-calibrated validation
113 data, reaching up to a factor of two (Zhu et al., 2016; Zhu et al., 2019b). Therefore, before
114 inverse modelling estimates can be used to supplement bottom-up emission inventories, an
115 assessment of their reliability and associated uncertainty over diverse regions is needed.

116 The main goal of this study is to provide a comprehensive, systematic comparison of emission
117 estimates derived from inverse modelling techniques for various species (CO, NOx, NMVOC,
118 SO_2, BC, and OC) to current state-of-the-art emission inventories for several regions of the
119 world. To this end, we compiled estimates of anthropogenic emissions from eleven different
120 sources based on various inverse methods. These estimates are compared to the most widely
121 used global inventories EDGARv4.3.2 (Crippa et al., 2018) and CEDS (Hoesly et al., 2018), as
122 well as to recent regional inventories for Europe (CAMS-REG-AP, Granier et al. 2019), Africa
123 (DACCIWA, https://www.eccad3.sedoo.fr) and China (MEICv1.3: http://www.meicmodel.org,
124 Zheng et al., 2018).
125

Another objective is to compare the trends in the projected emissions of the Shared Socioeconomic Pathways (SSPs) developed for the sixth Climate Model Intercomparison Project (CMIP6) (Riahi et al. 2017; Kreigler et al. 2012) to the current best estimates of emission trends for the recent past in selected regions. We aim to evaluate which narrative describes best the direction taken by the different regions in terms of emissions. Assessing how well the scenarios capture recent emission trends will be useful for determining their suitability for studies that evaluate emissions in the recent past and near future, such as pollution control/mitigation impact studies and air quality forecasting. Furthermore, we compare CO and NOx emissions from the SSPs to those of the Representative Concentration Pathways (RCPs) that were used in the fifth Climate Model Intercomparison Project (CMIP5) (Moss et al. 2010; van Vuuren et al, 2011) for several world regions. While a comprehensive overview of the SSP emissions and comparison with the RCPs is presented in Gidden et al. (2019), we are focused on the regional scale, and intend to aid in the interpretation and analysis of regional climate change studies.

2 Materials and Methods

This study compares 10 different top-down emission estimates to several state-of-the-art global and regional bottom-up inventories for CO, NO_x, NMVOC, SO_2, OC and BC. A description of each of the top-down estimates is provided below. Details and references for each of the top-down and bottom-up inventories are also given in Tables 1 and 2, respectively. We focus on the following 12 regions as defined by the IMAGE2.4 26 regions (Bouwman et al., 2006): China, the Middle East, Western Africa, the United States, Western and Central Europe, South America, India+, Southeast Asia, Indonesia+, Oceania and Southern Africa. Note that India+ includes neighbouring countries such as Pakistan, Afghanistan, Nepal, and Bangladesh. A map of the regions is shown in Figure 1. These regions were selected based their economic and geographic diversity, as well as on the availability of top-down and bottom-up regional inventories. The regional averages for all datasets are calculated on their native grids.

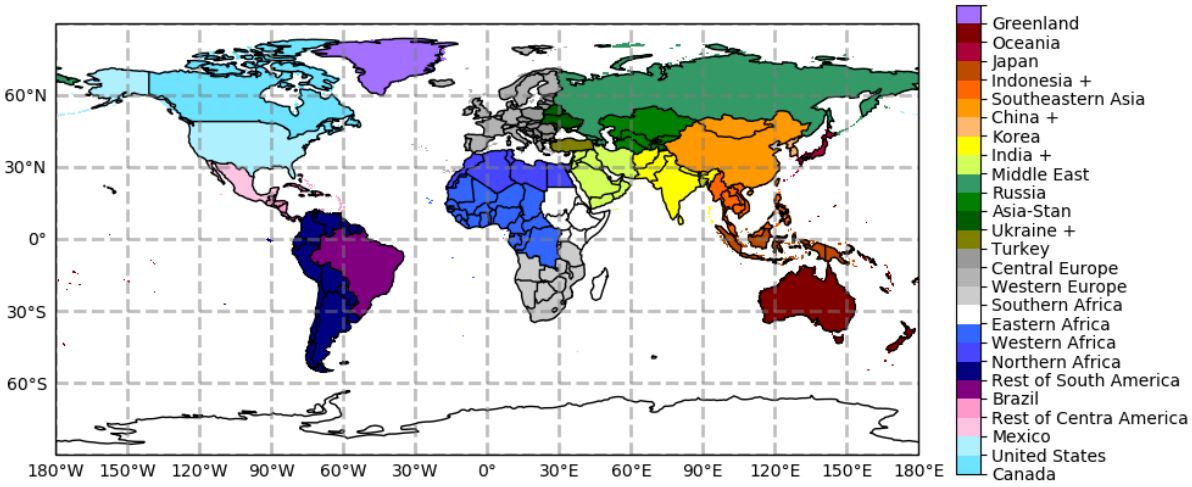

Figure 1: This study focuses on the following 11 regions as defined by Bouwman et al. (2006), the Middle East, Western Africa, the United States, Western and Central Europe, South America, India+, Southeast Asia, Indonesia+, Oceania and Southern Africa, plus China which only includes the national boundaries.

2.1 Calculation of trends and percent differences

We evaluate recent trends in emissions from the five SSPs based on the years 2010-2020. The trends are derived from ordinary linear regression and expressed in units of percent change per year relative to the mean over the data period. The SSP trends are compared to trends which are based on the emissions from the inventories and inversion estimates. These trend estimates are calculated by averaging the trends from all available inventories for a particular region, including all inverse modelling estimates and bottom-up inventories which are available from 2010 until at least 2015 which are statistically significant ($p > 0.05$). A list of the individual trends is provided in supplementary material. Note that MACCity and CAMS-GLOB-ANT are excluded because their recent years are based on projections of past trends from inventories and are therefore not considered independent. Unless otherwise specified, percentage differences in the range of emission estimates are calculated based on the average between the highest and lowest values.

3 Data

3.1 Top-down Emissions

174 ***Global***

175

176 ***Chen et al. (2019)***: Global daily carbonaceous aerosol (OC and BC) emissions for the period
177 2006-2011 are derived using the GEOS-Chem adjoint model (Henze et al., 2007) at a spatial
178 resolution of 2.5°x2° (Chen et al., 2019). OC and BC emission sources are constrained using
179 retrievals of aerosol optical depth (AOD) and aerosol absorption optical depth (AAOD) (Chen et
180 al. 2018, 2019) from the multi-angular and polarimetric POLDER/PARASOL (Polarization &
181 Anisotropy of Reflectances for Atmospheric Sciences coupled with Observations from a Lidar)
182 measurements retrieved via the GRASP (General Retrieval of Atmosphere and Surface
183 Properties) algorithm (www.grasp-open.com) (Dubovik et al., 2011, 2014). Note that the
184 anthropogenic contribution of the total derived black and organic carbon emissions is estimated
185 based on a ratio which is applied in the GEOS-Chem (v10-1) model.

186

187 ***Jiang et al (2017)***: Global CO emissions are constrained over the period 2001-2015 by
188 assimilating multi-spectral CO measurements from MOPITT (version 6) using the 4D-Var data
189 assimilation system (adjoint) in the GEOS-Chem model at a spatial resolution of 5°x4°. The
190 initial conditions and land boundary conditions (CO concentrations) are optimized using a
191 sequential sub-optimal Kalman filter. Here we include two of the inversions described in Jiang et
192 al. (2017), one in which emissions are constrained using MOPITT CO profiles and another using
193 total CO columns. Anthropogenic CO emissions are separated from other sources using a single
194 scaling factor, based on the a priori emissions, to adjust all emissions in a grid.

195

196 ***Tropospheric Chemistry Reanalysis (TCR-2)***: Global NO_x and SO_2 emissions are constrained
197 over the period of 2005-2018 by assimilating multiple satellite data sets for multiple species
198 (NO_2, CO, O_3, SO_2) using the global CTM (Chemistry Transport Model) MIROC-Chem
199 (Watanabe, et al., 2011) based on the ensemble Kalman filter (EnKF) technique performed at
200 1.125° × 1.125° resolution in the TCR-2 framework (Miyazaki et al. 2017, 2019, 2020a, 2020b).
201 The assimilated measurements were obtained from OMI (the Ozone Monitoring Instrument),
202 GOME-2 (Global Ozone Monitoring Experiment–2) and SCIAMACHY (SCanning Imaging
203 Absorption SpectroMeter for Atmospheric CHartography) for NO_2, TES for O_3, MOPITT for
204 CO, and MLS for O_3 and HNO_3, and OMI for SO_2.

***Müller et al. (2018)*:** Global CO emissions for 2013 are derived at 2° × 2.5° resolution based on the adjoint of the IMAGESv2 model constrained by satellite IASI CO column data. The model uses prescribed OH fields constrained by methylchloroform measurements. An ensemble of top-down simulations is carried out and the top-down emissions are compared with various independent CO observations and evaluated. The inversion adopting the lowest average OH level in the Northern Hemisphere provides the best agreement with all tested independent observation data sets, and the corresponding top-down emissions are used in our study. Emissions are derived for three categories (anthropogenic, biogenic and biomass burning) using a technique which relies on the spatio-temporal patterns of the a priori emissions, through assumed correlations between a priori emission errors. In essence, the inversion tries to preserve the patterns of the a priori. The strength of that constraint is determined by the assumed correlations.

***Zheng et al. (2019)*:** Global CO emissions for the period 2000-2017 are derived using the global 3-D transport model of the Laboratoire de Météorologie Dynamique (LMDz) coupled with a simplified chemistry module, Simplified Atmospheric Chemistry assimilation System (SACS) based on a multi-species atmospheric Bayesian inversion approach (Zheng et al., 2018a, 2018b) at a spatial resolution of 3.75°×1.9°. Zheng et al. (2019) perform the following three global inversions which are used in this study: (i) an inversion constrained only by CO total column data from the MOPITT version 7 over 2000-2017 (inversion 1); (ii) an inversion also constrained by HCHO column data from Ozone Monitoring Instrument (OMI) version 3 on the basis of inversion 1 for the period 2005-2017(inversion2); (iii) an inversion further constrained by column-averaged dry air mole fractions of CH_4 (XCH_4) from Greenhouse gases Observing SATellite (GOSAT) on the basis of inversion 2 for the period 2010-2017 (inversion 3). Emissions are derived for four categories (anthropogenic, biomass burning, biogenic and oceanic) by multiplying the optimized 8-daily surface CO total fluxes by the proportion of each sector in each model grid cell as given by the prior.

Regional

236 ***Cao et al. (2018):*** NMVOC emissions in China for the year 2007 are derived using the GEOS-
237 Chem CTM (version 8.2.1) and its adjoint at a spatial resolution of 5° × 4°). The GEOS-Chem
238 CTM was updated to include improved NMVOC chemical schemes. Emissions are constrained
239 by using HCHO and glyoxal columns observed by the GOME-2A and OMI satellite instruments.
240 Four inversion experiments using different combinations of these satellite observations were
241 conducted in order to explore their impacts on the top-down emission estimates. The
242 anthropogenic NMVOC emission estimates for 2007 range from 16.4-23.6 Tg yr^{-1}. In this study,
243 we show the average of the four estimates which is 20.2 Tg yr^{-1}.
244
245 ***Qu et al. (2019a)***: NO_x and SO_2 emissions in East Asia for the period 2005-2012 are derived
246 simultaneously using the GEOS-Chem adjoint model (Henze et al. 2007, 2009) and a hybrid 4D-
247 Var / mass balance approach at 0.5° × 0.667° resolution (Qu et al., 2017). The emissions are
248 constrained by the OMI NO_2 NASA standard product (Krotkov et al., 2017) and the OMI Royal
249 Belgian Institute for Space Aeronomy (BIRA) SO_2 product (Theys et al., 2015). We refer to this
250 inventory as Qu-joint. An inversion is also performed constraining only NO_2 in order to assess
251 the benefits of constraining multiple species. This inversion is referred to as Qu-single. The
252 inversions were performed on a limited domain which does not included all of the countries of
253 the India+ region shown in Figure 1 of the Supplement, therefore the averages for Qu-single and
254 Qu-joint are for India only.
255
256 ***Qu et al. (2019b)***: Global SO_2 emissions for the period 2005-2017 are derived using the GEOS-
257 Chem adjoint model (Henze et al. 2007, 2009) and a hybrid 4D-Var / mass balance approach at a
258 2° × 2.5° horizontal resolution. In order to assess the uncertainty related to satellite retrievals,
259 two inversions are performed using different OMI satellite retrievals to constrain the emissions;
260 the NASA standard product OMSO2 (Li et al., 2013) and the BIRA product (Theys et al., 2015).
261 Note that these SO_2 emissions are shown only for China and India because the estimates are less
262 accurate in comparatively cleaner areas with lower SO2 columns due to negative column
263 densities in the OMI SO_2 retrievals (Qu et al., 2019). These inversions are referred to as Qu-
264 BIRA and Qu-NASA.
265

Stavrakou et al. (2017): Global NMVOC emissions for the period 2005-2014 are derived using the adjoint model technique in the IMAGESv2 global CTM at a spatial resolution of 2° × 2.5°. Emissions from open fire vegetation and human activities are constrained using vertical columns of formaldehyde (HCHO) retrieved from the Ozone Monitoring Instrument (OMI-BIRA). The anthropogenic VOC sources are found to be weakly constrained by the inversions on a global scale due to their small contribution to the total HCHO columns (Stavrakou et al. 2009), except over strongly polluted regions, like China.

Table 1: Description of inverse modelling estimates considered in this study.

	Species	*Region*	*Res. (lon x lat)*	*Period*	*CTM*	*Satellite constraint*	*Inversion method*
Global							
Chen et al. (2019)	OC/BC	Global	2.5° x 2°	2006-2011	GEOS-Chem	PARASOL/ GRASP* AOD/AAOD	Adjoint
TCR-2	NO_x	Global	2.8° x 2.8°	2005-2018	MIROC-Chem	OMI/GOME-2/SCIAMACHY NO_2,TES O_3, MOPITT CO, MLS O_3/HNO_3	Ensemble Kalman filter
Müller et al. (2018)	CO	Global	2.5 ° x 2°	2013	IMAGESv2	IASI CO and OH levels based on methylchloroform (MCF) obs.	Adjoint
Zheng et al. (2019)	CO	Global	3.75° x 1.9°	2000-2017	LMDz-SACS	MOPITT CO, OMI HCHO, GOSAT XCH4	Bayesian
Jiang et al. (2017)	CO	Global	5° x 4°	2001-2015	GEOS-Chem	MOPITT CO and OH levels based on MCF obs.	Adjoint
Regional							
Cao et al. (2018)	NMVOC	China	5° x 4°	2007	GEOS-Chem	GOME-2/OMI HCHO/ CHOCHO	Adjoint
Qu et al. (2019a)	NOx, SO_2	East Asia	0.5° x 0.667°	2005-2012	GEOS-Chem	OMI SO_2, NO_2	Adjoint
Qu et al. (2019b)	NOx	East Asia	2.5° x 2°	2005-2017	GEOS-Chem	OMI NO_2	Adjoint
Stavrakou et al. (2017)	NMVOC	China	2.5 ° x 2°	2005-2014	IMAGESv2	OMI HCHO	Adjoint

3.2 Bottom-up Emissions

279 In this study we compare 13 of the most recent anthropogenic global and regional bottom-up
280 inventories, respectively. Included in the global inventories are EDGARv4.3.2 (JRC, Crippa et
281 al., 2018) and CEDS (Hoesly et al., 2018) which are both traditional bottom-up inventories. We
282 also compare CAMS-GLOB-ANTv4.1 and MACCity which are based on bottom-up inventories
283 and projections, thereby provide emissions to the current year. The CAMS global emissions are
284 based on both the EDGARv4.3.2 and CEDS emissions. The standard version of CAMS-GLOB-
285 ANT (version 4.1) used in this study applies the monthly profiles provided by CAMS-GLOB-
286 TEMPO (Granier et al., 2019) to the annual emissions from EDGARv4.3.2 for the years 2000-
287 2012. After 2012, the data are linearly extrapolated to 2020 using trends derived from the CEDS
288 emissions for the years 2011-2014. A detailed description of all the global and regional bottom-
289 up inventories are presented in the Supplement, along with a brief discussion regarding the
290 uncertainties among global inventories.
291
292 **Table 2**: Description of global and regional bottom-up inventories considered in this study.

	Species	*Region*	*Res. (lon x lat)*	*Period*	*Reference*
Global Inventories					
CAMS-GLOB-ANT	NO_x, CO, NMVOC, SO_2, OC, BC	Global	0.1° x 0.1°	2000-2019	Granier et al. (2019)
EDGARv4.3.)	NO_x, CO, NMVOC, SO_2, OC, BC	Global	0.1° x 0.1°	1970-2012	Crippa et al. (2018)
CEDS	NO_x, CO, NMVOC, SO_2, OC, BC	Global	0.5 ° x 0.5°	1950-2014	Hosley et al. (2018)
HTAPv2	NO_x, CO, NMVOC, SO_2, OC, BC	Global	0.1° x 0.1°	2008, 2010	http://www.htap.org
MACCity	NO_x, CO, NMVOC, SO_2, OC, BC	Global	0.5 ° x 0.5°	2007	https://eccad3.sedoo.fr
Regional Inventories					
CAMS-REG-AP	NO_x, CO, NMVOC, SO_2, OC, BC	Europe	0.1° x 0.05°	2000-2017	Kuenen et al. (2014) Granier et al. (2019)
DACCIWA	NO_x, CO, NMVOC,	Africa	0.1° x 0.1°	2000-2015	Keita et al. (2020)

	SO_2, OC, BC				
DICE-Africa	NO_x, CO, NMVOC, SO_2, OC, BC	Africa	0.1° x 0.1°	2000-2015	Marais et al. (2016)
US NEI	NO_x, CO, NMVOC, SO_2	United States		2000-2016	https://www.epa.gov/air-emissions-inventories
MEICv1.3	NO_x, CO, NMVOC, SO_2, OC, BC	China	0.25 ° x 0.25°	2008-2017	http://www.meicmodel.org Zheng et al. (2018)
REASv3.1	NO_x, CO, NMVOC, SO_2, OC, BC	Asia	0.25 ° x 0.25°	1950-2015	Kurokawa et al. (2019)
Sharma et al. (2019)	NO_x, CO, NMVOC, SO_2	India		2011	Sharma et al. (2019)
Sun et al. (2018)	NO_x, CO, NMVOC, SO_2	China		1949-2015	Sun et al. (2018)

3.3 Shared Socioeconomic Pathways (SSPs)

The projected emissions from five SSPs were developed for use in the current Coupled Model Intercomparison Project phase 6 (Eyring et al., 2016). The SSPs are global scenarios which describe how the future emissions might evolve according to socioeconomic development, demographics, technological advances within the context of climate change mitigation and adaptation during the period 2015-2100 (van Vuuren et al., 2014; O'Neill et al., 2014; Kreigler et al., 2012). The air pollutant emission trajectories associated with the SSP scenarios have been harmonized with the CEDS historical global inventory for the year 2015 and are described in Rao et al., (2017) and Gidden et al. (2019). The pathways are based on five narratives describing alternative socioeconomic developments. SSP1 and SSP5 assume strong pollution control scenarios, and therefore emissions which are substantially lower than current levels, whereas according to SSP3 and SSP4 future emissions are higher than current levels. SSP2 is based on a medium pollution control scenario where emissions remain close to current levels (Rao et al. 2017). In addition, mitigation policies are added to each scenario in order to achieve a prescribed radiative forcing by the end of the 21st century (i.e. 2.6, 4.5, 6.0 and 8.5 W m^{-2}).

In this study, we focus on the four Tier 1 SSPs (SSP126, SSP245, SSP370 and SSP585), which have the same radiative forcing as the RCPs used in CMIP5, but combine socioeconomic and technological developments, and have been given priority in CMIP6 (O'Neill et al., 2016). In addition, we also analyze SSP460, which has been designated as a Tier 2 scenario in order to complement and extend the Tier 1 scenarios and the RCPs (O'Neill et al., 2016). The emissions associated with these scenarios are available at a 0.5° × 0.5° spatial resolution (https://esgf-node.llnl.gov/projects/input4mips).

4 Comparison of emission inventories and inverse modelling estimates

In this section, we compare inverse modelling anthropogenic emission estimates of CO, NO_x NMVOC, SO_2, BC and OC to global and regional inventories which were developed using bottom-up estimation methods over the six regions of interest described in Section 2 and shown in Figure 1.

4.1 CO

The annual average CO emissions for each region are displayed in Figure 2. The inversion estimates are shown for Zheng et al. (2019), Müller et al. (2018) and Jiang et al. (2017). We compare two estimates from Zheng; Inv1 which uses satellite constraints of only columns of CO for the time period 2000-2017, and Inv2 which, in addition, is constrained by both CO and HCHO columns for 2005-2017. Two estimates from Jiang et al. (2017) are also compared; Jiang-prof which assimilates profile data and Jiang-colm which assimilates total column data. More specific details can be found in the Supplement.

In regions with high emissions such as China, the U.S. and India, the inversion estimates are generally within the range of the bottom-up inventories in terms of magnitude and have a similar range of uncertainty. In all regions, Müller's estimates are significantly lower compared to those of Zheng or Jiang. The lower estimates of Müller et al. (2018) are due to the use of prescribed modelled OH levels which are based on observations of methylchloroform (MCF) and further modulated based on comparisons with aircraft profiles and ground-based data. The OH field prescribed in their inversion setup is at the lower end of the range of what has been reported in the literature and calculated in most CTMs, implying less CO oxidation. The resulting higher CO lifetime is in turn compensated by lower optimized emissions. Another factor which could partially explain the discrepancy among the top-down estimates is the satellite data used in the

inversion system. Müller assimilates IASI satellite CO data, while Zheng and Jiang, both of which have higher values, use MOPITT.

In Western and Central Europe, Müller's estimate for 2013 is within the narrow range of CO emission reported by the bottom-up inventories, and is quite close to the regional CAMS-REG inventory (Figure 2). However, regarding the U.S., Müller's estimate of CO emission is considerably below (approx. 35%) the regional U.S. EPA inventory. Müller et al. (2018) attribute this large discrepancy to an overestimation in the U.S. bottom-up inventory, which has also been suggested in other studies (Hudman et al., 2008; Anderson et al., 2014; Jiang et al., 2015). In other regions such as China, India and Western Africa, it is difficult to comment on the accuracy of the magnitude of the inversion (or bottom-up) emission estimates due to the lack of measurements and regional information.

The two inversion estimates of CO emissions from Zheng are quite similar in magnitude and trend in most regions, but differ in terms of inter-annual variability (Figure 2). The two estimates from Jiang show similar trends, but significant differences in magnitude over most regions, indicating that the type of data assimilated (e.g. profile vs. total column) has a large impact on the emission estimates. In most regions, the Jiang-prof estimates are higher than Jiang-colm. In China, there is a sharp decline in emissions after 2010 as a result of the stringent clean air policies that have been implemented in recent years due to the severe air quality issues which have been documented in other studies (Zheng et al., 2018). With the exception of the regional inventories MEIC v1.3 and REASv3.1, which show a decrease of 4.4 and 2.7 % yr^{-1} for the period 2011-2015, most of the inventories do not show the declining CO emissions after 2010. However, this trend is captured quite well by all of the inversion estimates which show a decrease in emissions ranging from 1 to 3 % yr^{-1} over 2010-2015. While both of Zheng's estimates capture the magnitude and decreasing trend in China after 2011, Inv1 stabilizes after 2014, whereas Inv2 continues to show a declining trend similar to the MEICv1.3 emissions. Between 2011 and 2017, the Inv2 estimates decrease at an annual rate of 5.6%, while the Inv1 estimates decrease at a slower rate of 3.3%. The only difference between these two inversions is that, in addition to constraining columns of CO, formaldehyde (HCHO) is also constrained in Inv2. Constraining HCHO has a significant influence on the chemical production of CO and the

trend in Inv2. Tropospheric columns of OMI HCHO have been reported to keep increasing over China, likely due to significant increases in NMVOC emissions (Shen et al., 2019; Li et al., 2019). This could explain why CO emission estimates continue to decrease in Inv2, while Inv1 flattens out since the optimized emissions are overestimated to compensate for the underestimation of CO photochemical production.

In the U.S., the CO inversion estimates from Zheng and Jiang are similar to the U.S. NEI regional inventory in terms of trends, and slightly higher in magnitude (Figure 2). Both estimates follow the continuing decreasing trend of the regional inventory up to 2010, after which Jiang's estimates diverge and indicate a stabilization in CO emissions in the United States. Jiang et al. (2017) attribute this slowdown of U.S. pollutant reduction to factors such as diminished returns on improved catalytic converters which they suggest are unaccounted for in the U.S. inventory (Jiang et al., 2018). Jiang et al. (2018) demonstrate that satellite retrievals and surface measurements also indicate a significant reduction in the decreasing trends of CO and NO_x concentrations after 2010 as compared to the previous years, corroborating the trend shown in their CO inverse estimates. However, there is not always a direct linear relationship between anthropogenic NO_x emissions and measurements of tropospheric NO_2. This point is further discussed in the following section on NO_x emissions.

In Europe, Zheng's CO inversion estimates match fairly well the general trends from the bottom-up inventories, which show a steady declining trend from the year 2000 that slows down after 2009. Zheng's estimates show a lot of inter-annual variability, while Jiang's estimates show higher emissions in 2015 than in 2009, indicating a slightly positive recent trend that is contrary to the inventories. In terms of magnitude of emissions, all of the inversion estimates are considerably higher, except for that of Müller which is very to the CAMS-REG-AP regional inventory as discussed above (Figure 2). Zheng et al. (2019) suggest that the bottom-up inventories underestimate emissions in these regions, and show that their model biases are reduced compared to independent ground-based CO measurement when the posterior emissions are used. However, given that Europe is a region where there is a relatively a high level of detailed emission information, the higher inverse estimates of Zheng and Jiang may be due to higher OH levels in their model, since the estimates by Müller et al. (2018), using

methylchloroform-constrained OH abundances, provide an excellent agreement with the bottom-up inventories.

The largest uncertainly among the inversion estimates is found In Western Africa, where the CO emissions range from 17 Tg (Jiang-colm) to 64 Tg (Zheng-Inv2) in 2010 (Figure 2). However, Jiang's estimates are likely biased towards the low-end because they are influenced by the low a priori emissions used in their inversion method. The scheme used to partition emissions into separate categories (e.g. anthropogenic, biomass burning, etc.) is different in each inversion system (see the Supplement and references therein) and based on information from the a priori emissions. Therefore, this can account for small differences between inversion estimates, particularly in regions such as Western Africa where there is a large contribution from non-anthropogenic sources, such as biomass burning. In addition, the data used to construct bottom-up inventories (e.g. emission factors, activity data, etc) in Africa also have quite large uncertainties. The DACCIWA and DICE-Africa regional inventories both show similar increasing trends in CO emissions. The DACCIWA estimate is about 33% higher than DICE-Africa in 2010, however, there are some sectors not included in DICE-Africa (e.g. on-grid energy and formal industry, see the Supplement for details) which accounts, at least in part, for the discrepancy.

In India, the inversion estimates are largely within the range of the global inventories and the regional inventory REASv3.1, however, they are almost twice as high as Sharma's estimate. The trends are similar to the inventories until about 2012, after which the inverse estimates begin to stabilize (Figure 2). Because India is one of the regions in which updated regional emission data is not easily available, it is difficult to evaluate the trend in CO emissions seen in the estimates. Although not shown here, Sharma projects a value of 53.9 Tg for the year 2021, indicating an increasing trend in CO emissions in India.

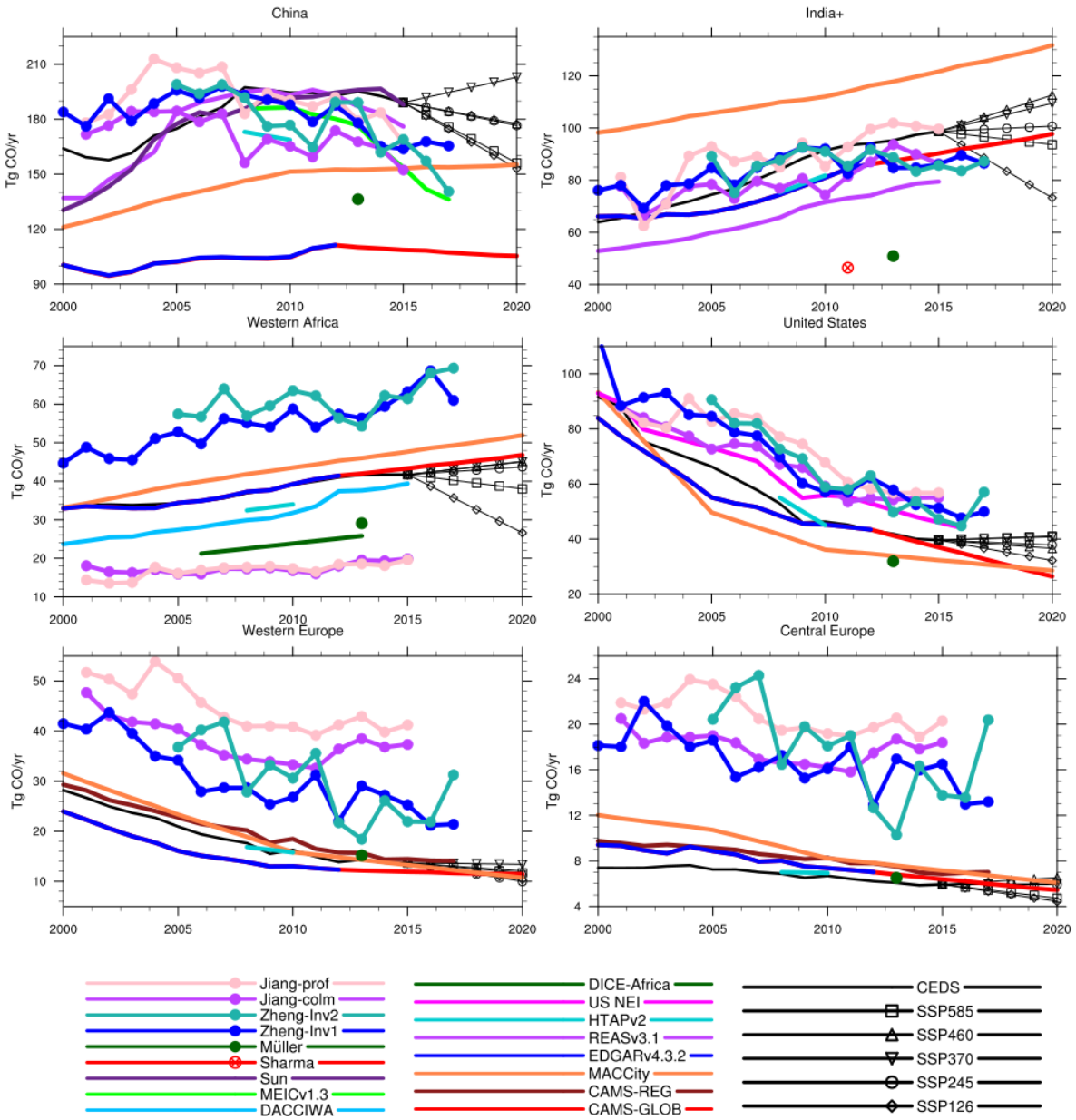

Figure 2. CO emissions from different inventories, inversion estimates and the SSPs. Note that the Sharma estimate is for the national boundaries of India only.

4.2 NOx

Figure 3 displays annually averaged NO_x emissions for each region. Inversion estimates are shown for TCR-2 in all regions and Qu in China and India. Two estimates for Qu are both derived using the same hybrid 4D-Var / mass balance inversion method. The 'single' estimates are constrained by only NO_2 observations and the 'joint' estimates are constrained by NO_2 and SO_2, as described in section 2. We recall from Section 2 that Qu's joint and single estimates are

for India only, while the TCR-2 and inventory emission averages are for India+ (Figure 1 in the Supplement) which is a larger region encompassing neighboring countries such as Pakistan, Nepal and Bangladesh. Qu's estimates would likely be 15-25% higher if they included India+. Although there is a slight difference in the magnitude between the 'single' and 'joint' species estimates, the results in China and India indicate that this difference is minor compared to the spread in the top-down emission estimates, at least at the regional scale. Qu et al. (2019a) report large differences at grid-scale, but not in the national budget between the 'single' and 'joint' inversions.

In terms of trends in NO_x emissions, the degree of agreement between the inversion estimates and the inventories varies regionally (Figure 3). In China, the trends are consistent with the regional inventories (MEICv1.3, REASv3.1 and Sun) and the CEDS global inventory, all of which show a broad peak around 2011-12, followed by a sharp decline. This declining trend is not found in the other global among the bottom-up inventories than the top-down estimates. For example, the Qu-single estimate for 2012 is the lowest of the inversion estimates (~17 Tg NO), while the TCR-2 estimate is about 25% higher (~21 Tg NO). Among the bottom-up inventories, CEDS is the highest (~23 Tg NO), about 45% higher than the lowest value given by Sun et al. (2018) (~16 Tg NOx). In China, the range of uncertainty is about 20% greater in the bottom-up emissions than the top-down emissions.

In the United States and Europe, the TCR-2 inversion estimates of NOx emissions generally follow the decreasing trends shown in the bottom-up inventories, except in recent years where TCR-2 shows a tendency towards a stabilization of emissions, while the inventories indicate a continuing significant decline (Figure 3). In the U.S. between 2010 and 2016, the TCR-2 NOx emissions decreased by about 3.8% per year on average, while the U.S. regional inventory shows a continuously strong reduction of almost 5.5% per year. Jiang et al. (2018) also report a slowdown of the decreasing trend in CO and NOx top-down emissions in the U.S. inferred by satellite NO_2 data and suggest that the method used to calculate the NEI U.S. emissions leads to an overestimation of the reduction of emissions after 2010, whereas an alternative fuel-based method could produce trends more consistent with the top-down estimates. Furthermore, the top-down emissions were found to be more consistent with observed ozone concentrations than

the U.S. inventory (He et al., 2019). In contrast, Silvern et al. (2019) assert that the continued decreasing trend in the U.S. national inventory is consistent with the trends in NO_2 surface observations, and that the stabilization in the OMI NO_2 trend, and the TCR-2 NO_x estimates, could be attributed to an underestimate of free tropospheric NO_2 background in the models. They suggest that increases in the relative contribution of non-anthropogenic background sources of NOx (e.g. lightning and soils) explains the discrepancy between trends in OMI NO2 and the NEI inventory. Furthermore, Li and Wang (2019) report that in rural areas, strong nonlinear relationships exist between anthropogenic NOx emissions and satellite NO_2 columns, implying that constraining NO_x emissions by only NO_2 satellite retrievals might lead to inaccurate estimates. Laughner and Cohen (2019) reported changes in NO_x lifetime for many U.S. cities and suggested that accounting for this change in lifetime more accurately (for example, by using models with higher resolution) should help to improve emission trend estimates. Clearly, a better understanding of the relationship between anthropogenic NO_x emissions and NO_2 satellite retrievals, as well as uncertainties in bottom-up methods used to estimate NO_x emissions, is urgently needed.

In India and West Africa, the inversion estimates fall within the range of the inventories, but they show a weaker increasing trend than the inventories (Figure 3). For example, in Western Africa for the period 2005-2015, the TCR-2 estimates increase by slightly less than 1.5% yr^{-1}, while the regional inventory DACCIWA increases by more than 3.5% yr^{-1} and DICE-Africa increases by more than 2% yr^{-1} (2006-2013). Similarly, in India during the period 2010-2015 NOx emissions given by REASv3.1 increase by almost 5% yr^{-1}, while the TCR-2 estimates increase at a slower rate of about 2.5% yr^{-1}. In 2011, the TCR-2 estimates 7.9 Tg NO_x which is in very good agreement with Sharma's value of 7.6 Tg NO_x.

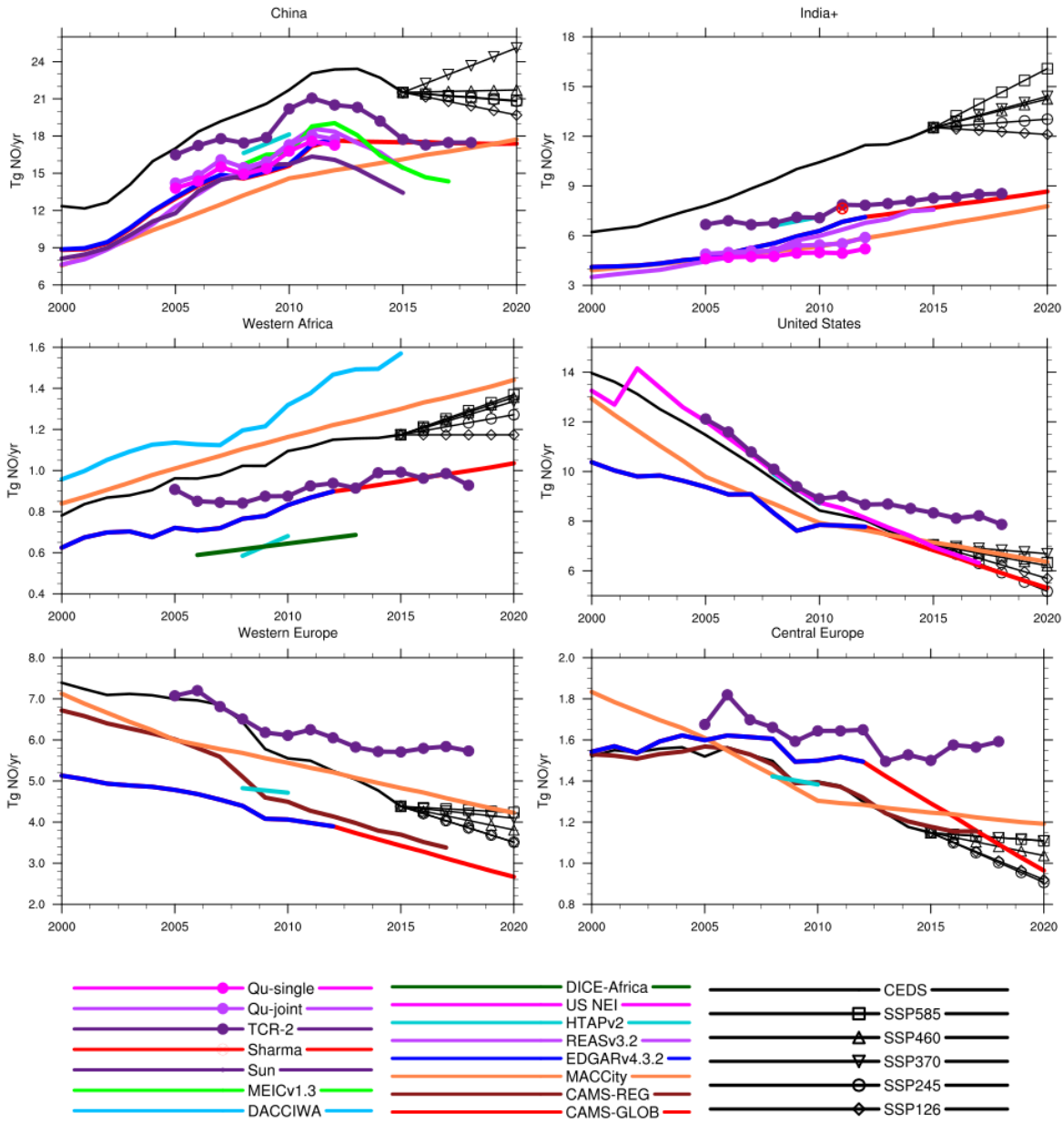

Figure 3. NOx emissions from different inventories, inversion estimates and the SSPs. Note that the Sharma estimate is for the national boundaries of India only.

4.3 NMVOCs, SO_2 and Carbonaceous Aerosols

Fewer inventories and inverse estimates are available for these species compared to CO and NOx. Figure 4a,b shows the annually averaged NMVOC inversion emission estimates in China from Stavrakou and Cao, along with the global and regional inventories. Note that Cao's estimate in Figure 3 represents an average of four inversion experiments, ranging from 16.4 to 23.6 Tg NMVOC, using different combinations of satellite observations as described in Cao et

al. (2018). The significant spread reflects uncertainty in the satellite data and its impact on top-down NMVOC estimates. Both the inversion estimates (Stavrakou and Cao) and the inventories lie within a narrow range (Figures 2 and 3), although this does not necessarily indicate less uncertainty. Cao's estimate for 2007 (20.2 Tg NMVOC) is slightly below the range of the inventories (21.0-27.5 Tg NMVOC) and is quite close to the REASv3.1 estimate for 2013 (21.0 Tg NMVOC). Stavrakou's estimates are similar in magnitude to the inventories and exhibit a stronger interannual variability. The inventories show an increasing trend in NMVOC emissions in China until ca. 2012, after which they start to level out. Over 2005-2014, Stavrakou's estimates indicate a weak positive trend of ca. 1.4% yr^{-1}, which is lower than those of REASv3.1 (5.2% yr^{-1} over 2005-2014), Li et al. (3.2% yr^{-1}) and MEICv1.3 (3.4% yr^{-1} over 2008-2014). The top-down emission trend is primarily driven by the tropospheric HCHO column trend, amounting to 1.3% yr^{-1} over Northern China between 2005 and 2014 (Stavrakou et al., 2017). Note that Shen et al. (2019) recently reported comparable summertime HCHO trends over Northern China over 2005-2016, and they found a good consistency with corresponding HCHO trends calculated by the GEOS-Chem CTM driven by MEICv1.3 emissions. The reasons for the apparent discrepancy with Stavrakou's results are unclear but might be related to intermodel differences.

Annually averaged SO_2 emissions for China and India are illustrated in Figure 4c,d with inversion estimates from Qu and TCR-2 for both regions. The two estimates from Qu are derived using identical methods, except the emissions are constrained using different OMI satellite retrievals (Qu-BIRA and Qu-NASA, Qu et al., 2019). The impact of the two different retrievals on the magnitude of emissions is more significant in China where the average difference in annual SO_2 emission estimates is about 20%. In India, this difference is around 6%, a consequence of the fact that differences in the satellite retrievals are not the same in all regions. Both estimates indicate relatively similar trends in China and India between the two OMI SO_2 products. A third estimate of SO_2 emission from Qu (Qu-joint) was derived using satellite SO_2 and NO_2 constraints simultaneously, as described in section 2. We recall that the Qu-joint inversion estimates is for India only, unlike the other inversion and bottom-up estimates which are for India+. The Qu-joint estimate would be roughly 25% higher if it included India+.

In China, the range of SO_2 emissions is large in both the inversion estimates and the bottom-up inventories (Figure 4c,d). For example, in 2010 the inversion estimates range from approximately 17 (TCR-2) to 24 (Qu-BIRA) Tg SO_2 and the inventories range from about 16 (Sun) to 28 (MEICv1.3) Tg SO_2. While the inversion estimates show a significant decrease in Chinese emissions after 2010, this decline is not as steep as in the regional REASv3.1 and MEICv1.3 inventories in which SO_2 emissions decreased by about 35 and 40% between 2011 and 2015, respectively. In general, the inversion estimates are significantly lower than in the regional inventories until after 2014.

In India, SO_2 emissions derived from the inversion systems are all considerably lower than what is reported in most inventories (Figure 4c,d). The exception is Sharma's bottom-up estimate for 2011 of 6.5 Tg SO_2 which is considerably lower than the other inventories and closer to the inversion estimates. Even if we add 25% to Sharma's estimates for India to account for the other countries included in the India+ region, it is still the less than the other bottom-up estimates. The inventories all indicate that emissions have been steadily increasing in India since about 2005, however, this trend is weaker in the inversion estimates. The weaker trends in the inversion estimates could in part be due to satellite sensors which are not sensitive enough to pick some of the diffuse sources. Posterior SO_2 emissions in less polluted areas are harder to estimate due to the large amount of negative retrievals (Qu et al., 2019).

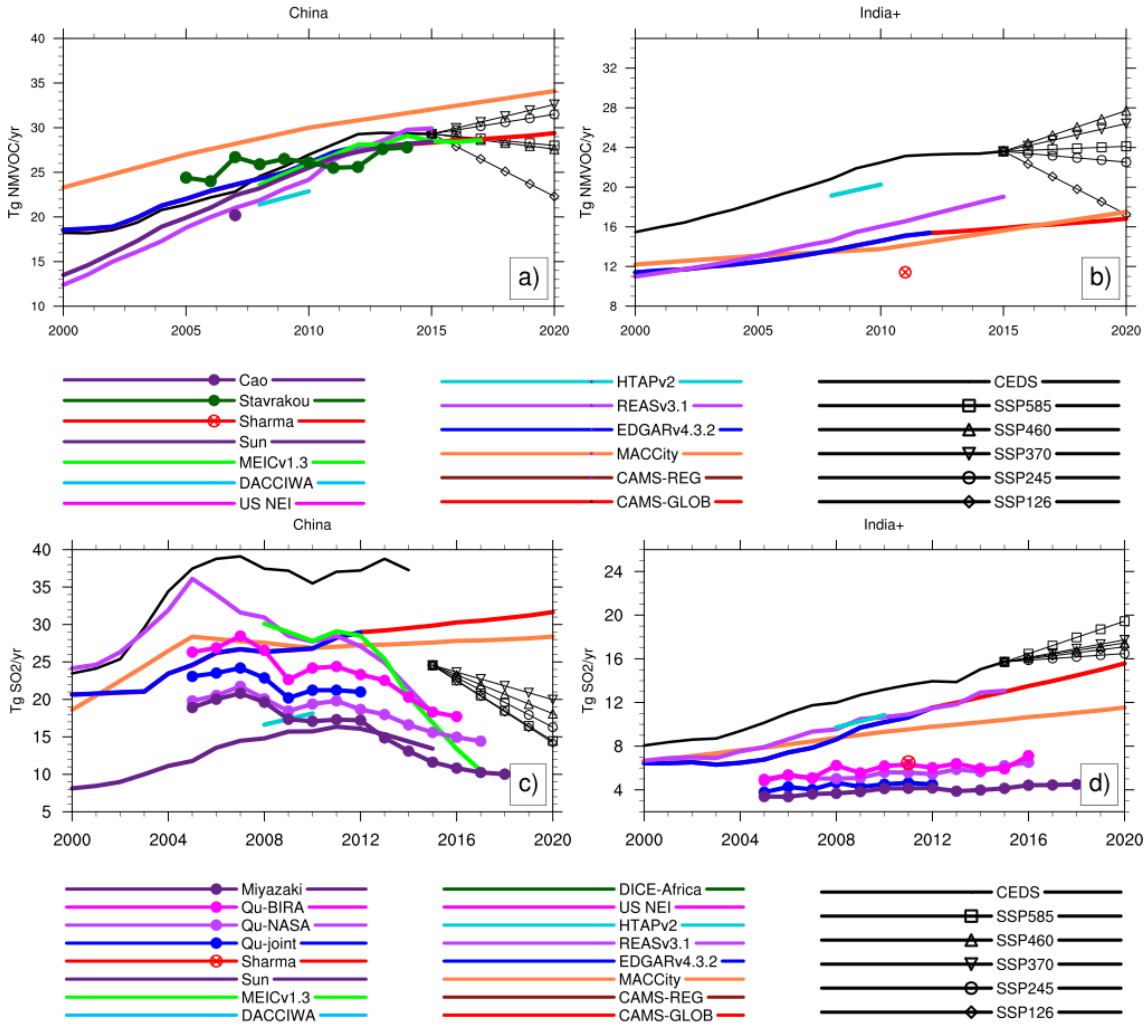

Figure 4. NMVOC (a, b) and SO2 (c,d) emissions from different inventories, inversion estimates and the SSPs. Note that the Qu-joint and Sharma estimates are for the national boundaries of India only.

Figure 5 shows annually averaged black and organic carbon emissions in China, India and Western Africa. Chen's inverse emission estimates provide a unique global time-series for the period 2006-2011, as a first attempt in using an inversion approach to indirectly derive black and organic carbon emissions by fitting satellite measurements of spectral aerosol extinction (AOD) and absorption (AAOD) (Chen et al., 2019). The inversion estimates of BC emissions are within the range of the bottom-up inventories in China and Western Africa, and slightly below in India (Figure 5). In contrast, the inversion estimates of anthropogenic OC emissions are considerably higher than most inventories in China and Western Africa, and at the upper end of the range in

India. It is interesting to note that Chen's estimates and the DACCIWA regional inventory show considerably higher OC emissions than the global inventories and the regional inventory DICE-Africa, while BC emissions are quite similar. This could suggest an underestimation in OC emissions in the global inventories in these regions. Other studies have identified inaccuracies in global inventories in West Africa where there is much uncertainty related to the emission factors and activity data from region-specific emissions sources which are unaccounted for (Liousse et al., 2014; Marais et al., 2016). For example, wood burning for cooking and heating is a large source of OC and BC emissions in Africa but is likely misrepresented in inventories due to lack of representative data. Inversion estimates could potentially be used to improve inventory emissions from these and other misrepresented sources. However, uncertainties in the inversion estimation of black and organic carbon by fitting indirectly measurements of AOD/AAOD need to also be better quantified. Both the BC and OC inversion estimates show a stronger interannual variability than the bottom-up inventories, but in most cases the general trends agree reasonably well.

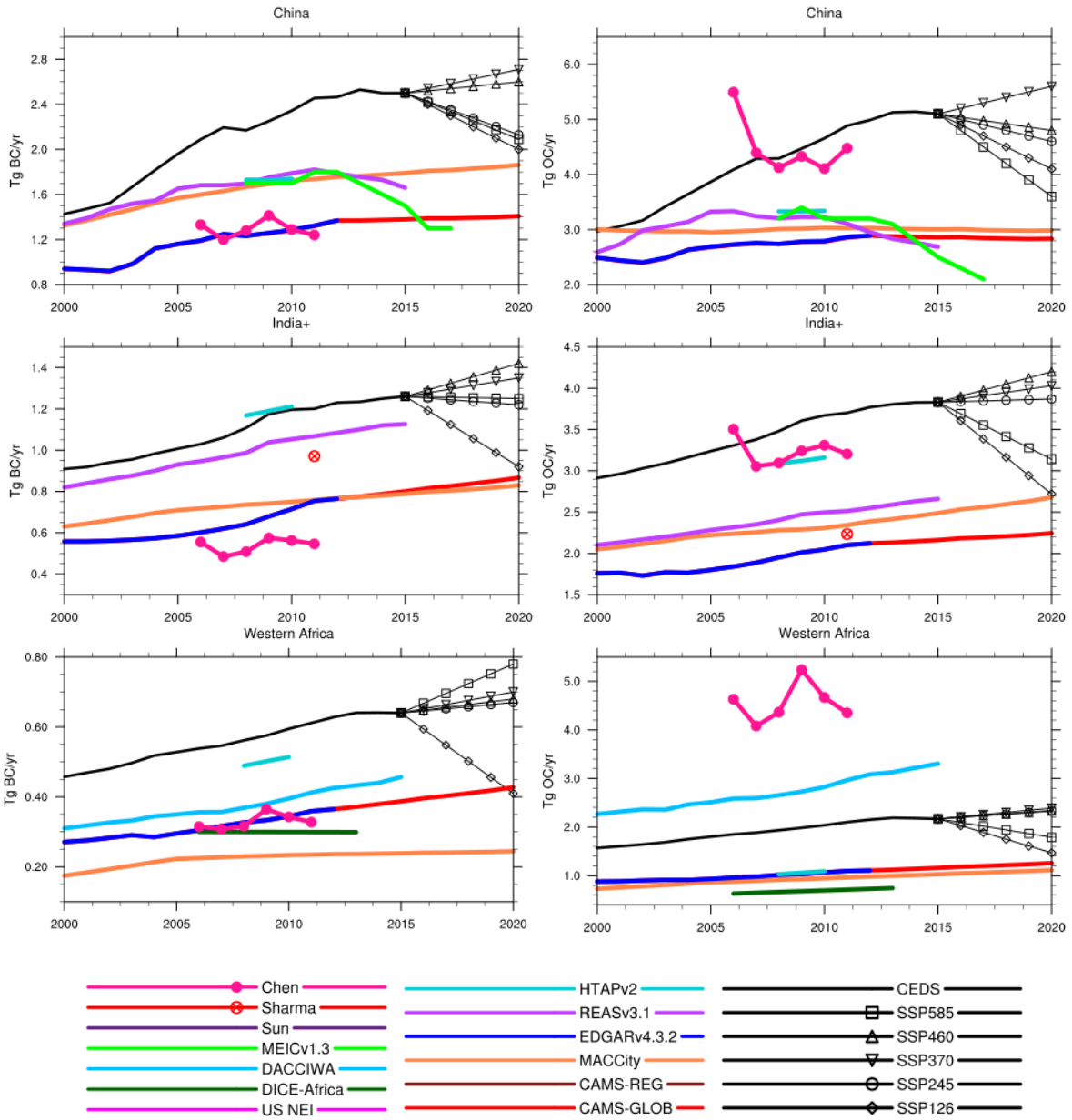

Figure 5. BC and OC emissions from different inventories, inversion estimates and the SSPs. Note that the Sharma estimate is for the national boundaries of India only.

5 Comparison of recent emission trends with SSPs for different regions

In this section, we compare recent trends from available inventories and inversion estimates to the five SSP scenarios under consideration. Linear trends of NOx and CO emissions from the SSPs for the years 2010-2020, and the average of the trends from the bottom-up inventories and inverse modelling estimates (INV) which have data until at least 2015, are summarized in Table 3. All trends are expressed in % yr^{-1} relative to the mean over the data period. Individual trends

and their statistical significance is given in supplementary material. Note that for CO INV trends, we include only the Zheng et al. (2019) estimates from the inversion using the most recent satellites constraints for CO, HCHO and CH_4 (inversion 3, cf. Section 2), and the Jiang-prof estimates which assimilates profile data. For each region, the SSP trends which differ by less than 1% compared to the INV trend are in bold, indicating the scenarios with recent trends that are closest to those of the inventories and inverse modelling emissions. This type of analysis is to a certain extent speculative, therefore the results only indicate suggestions of the scenarios which match most closely the estimations of actual recent trends. Furthermore, recent trends in the last 10 years are not necessarily indicative of how emissions will evolve in the future. Recall that SSP1 and SSP5 are both strong pollution control scenarios; SSP5 assumes an energy-intensive, fossil fuel based economy, while SSP1 represents a future shifted towards more sustainable practices. SSP3 and SSP4 represent futures with more pessimistic development trends, where there is little investment in health and education and fast growing populations. In SSP3, national and regional security is prioritized, whereas in SSP4 large inequalities dominate both within and across countries. SSP2 is the moderate pollution control scenario, in which trends more or less follow their historical patterns.

In China, SSP126 is the scenario which matches most closely to the actual recent trends in CO emissions. This is a strong pollution control scenario that reflects the stringent air quality standards China has enforced in recent years. All of the SSP NOx trends agree with the declining emissions reported by the inventories (REASv3.1, Sun, MEICv1.3) and inverse modelling estimates (Qu-joint, TCR-2 and DECSOv5.1qa), but for the period considered, 2010-2020, the decrease is not as strong. However, considering only the last few years since 2015, we can see in Figure 2 that the MEICv1.3 regional inventory and the inverse modelling estimates from DECSOv5.1qa both show a decline in the decreasing trend of NO_x emissions, which is qualitatively similar to that of SSP126.

The results indicate that recent emission trends in the United States are also similar to SSP126 (Table 3). The INV trends, which are based on the NEI regional inventory and inverse modelling estimates, show recent declines in NO_x and CO emissions on the order of 3% yr^{-1}, consistent with the strong pollution control scenario. However, it should also be noted that the CO

inversion estimates from Jiang et al. (2017) which show a slowdown in declining CO emissions in the US are not included in the INV average because there is not a statistically significant trend. If the Jiang et al. (2017) inversion estimates are included, the INV trend would show less of a negative trend in CO emissions more similar to that of SSP585. In Western and Central Europe, as in the U.S., there is a smaller spread in emissions among the SSPs, especially during the early century, therefore the trends are more similar and indicate the same sign. Trends from SSP126 and SSP585 match most closely to the INV trends for Europe, both of which are strong pollution control scenarios. However, it should be noted that the inversion estimates of CO (Jiang et al. (2017) and Zheng et al.(2019)) and NOx (TCR-2) emissions do not show a statistically significant trend in recent years in Europe, and therefore are not included in the INV trend average which is based largely on the CAMS-REG-AP regional inventory (Figures 1 and 2). In Southeast Asia, the strong pollution control scenario SSP126 also matches the INV trend most closely, which indicates a positive trend in NO_x and declining trend in CO emissions.

Our results, based on the trends given in Table 3 as well as a qualitative visual interpretation of Figures 1 and 2, indicate that the most likely scenario representing recent emission trends in India is SSP370 which is a low pollution control scenario. In Western Africa and Indonesia+, emission trends from SSP460 match most closely to the recent INV trends in NO_x and CO emissions. SSP4, also a low pollution control scenario, represents a scenario with a fast-growing population with increasing inequalities, leading to societies that are highly vulnerable to climate change. Indeed, air quality is deteriorating in many West African countries due to rapid increases in population, economic growth and coinciding lack of regulations, especially in megacities (Liousse et al. 2014). For some of the regions the results are ambiguous, either because none of the SSP emission trends are close to the actual trends (i.e. Southern Africa), or because there is not a statistically significant INV trend (i.e. Middle East and South America). In general, and especially in regions where there is a lack of reliable emission data, the results should be interpreted with caution in terms of robustness.

Table 3: Linear trends of NOx and CO emissions from SSPs for the years 2010-2020, and the averaged trend from all regional inventories and inversion estimates (INV) which have data until at least 2015 and are statistically significant ($p > 0.05$). Trends are expressed in units of % yr^{-1} relative to the mean over the data period. The number of available datasets with statistically significant trends used to calculate the average is indicated in parenthesis. SSP trends shown in bold correspond most closely to recent observed trends for NOx and CO.

		INV	SSP126	SSP245	SSP370	SSP460	SSP585	closest scenario
China	NO_x	**-3.07 (*4*)**	-1.59	-1.06	0.86	-0.64	-1.03	**SSP126**
	CO	**-2.94 (*3*)**	**-2.36**	-1.03	0.36	-0.98	**-2.19**	
Middle East	NO_x	*	0.02	0.44	1.29	-1.39	1.01	----
	CO	*	-2.12	-3.31	-0.12	-1.86	0.02	
Western Africa	NO_x	**+2.03 (*2*)**	0.59	1.40	**1.92**	**2.08**	2.18	**SSP460**
	CO	**+3.35 (*2*)**	-3.52	0.97	1.27	1.30	-0.41	
India	NO_x	**+3.33 (*2*)**	1.39	2.13	**3.17**	**3.05**	4.35	**SSP370**
	CO	**+1.32 (*3*)**	-2.03	**0.95**	**1.81**	2.10	0.23	
United States	NO_x	**-3.16 (*2*)**	-3.98	-4.80	-2.47	**-3.19**	**-2.99**	**SSP126**
	CO	**-3.70 (*3*)**	**-3.54**	-2.02	-1.28	-2.34	-1.21	
Western Europe	NO_x	**-2.47 (*2*)**	-4.86	-4.86	**-3.44**	-4.12	**-3.12**	**SSP126**
	CO	**-4.21 (*1*)**	**-3.87**	**-4.19**	-1.48	-2.50	-2.80	
Central Europe	NO_x	**-3.44 (*1*)**	**-4.21**	**-4.34**	-2.46	-3.11	-2.46	**SSP126**
	CO	**-3.20 (*1*)**	-3.72	-1.01	-0.93	-0.03	**-3.18**	
South America	NO_x	*	-0.07	-0.41	1.12	-0.52	0.94	---
	CO	*	-2.56	-2.85	-0.47	-1.31	-1.74	
Southeast Asia	NO_x	**+2.07 (*2*)**	**1.84**	0.45	2.07	2.00	**1.35**	**SSP126**
	CO	**-2.72 (*2*)**	**-3.02**	-0.97	1.05	0.84	-0.08	
Indonesia	NO_x	**+1.43 (*2*)**	0.61	0.08	2.01	**1.44**	**1.41**	**SSP460**
	CO	**+2.86 (*2*)**	-3.15	-1.83	0.50	0.65	-0.63	
Oceania	NO_x	*	-0.75	-0.38	0.36	-0.32	0.17	---
	CO	**-5.90 (*1*)**	-3.17	-1.07	-1.21	-2.08	-0.91	
Southern Africa	NO_x	**+2.91 (*1*)**	-0.19	0.21	0.76	0.32	0.32	---
	CO	**+3.04 (*2*)**	-2.53	0.80	1.11	1.28	-0.37	

673
674

6 Conclusions

In this study, we have presented a comprehensive overview and comparison of current state-of-the-art top-down and bottom-up emission estimates of CO, NO_x, NMVOC, SO_2, BC and OC for several world regions. The results show that the top-down estimates are generally within the range of bottom-up emission inventories and exhibit a similar level of uncertainty, or even less in certain regions such as China. In general, for all species the largest discrepancies are found outside of regions such as the U.S., Europe and Japan where the most accurate and detailed information on emissions (e.g. activity data, emission factors) is available. In terms of absolute magnitude, the largest spread in CO and NO_x inventory emissions is found in China where in 2010 differences are approximately 90 (~60%) and 6 (~33%) Tg, respectively. Significant differences are also seen for other compounds in China: ~20 Tg (~80%) for SO_2, 2 Tg (~55%) for OC, ~1 Tg (+55%) for BC. Contrarily, NMVOC inventory emissions are in better agreement in China, with a difference of ~4 Tg (~15%) in 2010, as compared to most other regions (e.g. ~8 Tg (~90%) in Western Africa and ~8 Tg (~45%) in India+). This agreement might be coincidental, however, and does not necessary imply that the emissions are less uncertain. In terms of percentage differences, the variation is not region- or species-dependent, and in general ranges from about 15% up to about 100%. In part, this likely reflects differences in the inclusion/exclusion of specific sectors, as well as in the methodologies used to construct the bottom-up inventories. A more in-depth detailed analysis at the sectoral level would give insight into how much of the uncertainty is due to these factors, but would be beyond the scope of this study.

696

Top-down emission estimates offer great potential and clear advantages, however, future work aimed at identifying, quantifying and reducing the uncertainties is needed.

Constraining multiple species in inversion modelling methods can lead to better consistency in simulated atmospheric chemical processes and thus more accurate optimized emissions (e.g., Zheng et al., 2019a; Qu et al., 2019a). Correctly modelling OH fields are also important due to its significant impact on oxidation processes (Müller et al., 2018; Jiang et al., 2011; Miyazaki et al., 2020b). More generally, the representation of chemical and transport processes in model

should be improved. In addition, the type of satellite data assimilated (e.g. profile vs total column) has a large impact on inversions (e.g., Jiang et al., 2017) and should be further explored. Finally, the satellite retrievals have important uncertainties with significant impacts on the emission inversions. Much can be learned in terms of quantifying these and other sources of uncertainty in inverse modelling estimates through more collaborated inter-comparison projects such as the Global Carbon Project (www.globalcarbonproject.org) which targets CO_2 and CH_4. A first step has been made with the IGAC AMIGO project (Analysis of eMIssions usinG Observations, https://amigo.aeronomie.be/) which brings together the international scientific community with the common goal of better quantifying emissions for a variety of trace gases and at different spatio-temporal scales. Inverse modelling has been identified as an integral part of AMIGO.

Top-down emissions offer great potential to supplement or improve bottom-up inventories, particularly in regions where global inventories often lack the necessary up-to-date and accurate information regarding regional activity data and emission factors. For example, China has undergone rapid economic growth in addition to stringent pollution control policies in recent years, both of which have led to rapidly changing activity data and emission factors (Zheng et al., 2018). This evolution has had a large impact on emissions, which were estimated to have been decreasing substantially in China during the last several years, except for NMVOC. The downward trend in China's emissions is well captured by the inversion estimates, as well as (Rao, et al., 2016)by the detailed regional inventories, but is not represented in any of the global inventories. This is a clear example of where inversion estimates provide useful constraints to the global bottom-up inventories, particularly in countries that are undergoing rapid changes in economy, technology, and environmental policies, such as India and Africa. Finally, since inversion estimates become available more quickly than bottom-up inventories, they can be used to extrapolate bottom-up inventories to the most recent years, which would benefit air quality forecasting. This also adds information that can be used to tune baseline emissions in recent years in the development of future emission scenarios such as the RCPs and SSPs.

This study has also compared recent emission trends in regional inventories and inversion estimates to those of five SSP near-future projections for several world regions. For each region,

we identified the scenarios for which the recent CO and NOx trends for the recent years (2010-2020) match most closely the best estimates based on bottom-up and top-down estimates. This type of analysis can be helpful in updating inventories for the most recent years and can serve as a guide in selecting CMIP6 climate change projections to be used for regional downscaling in air quality forecasting, and near-future pollution control/mitigation and climate impact studies. In addition, highlighting inconsistencies between the SSPs and actual emissions can help improve in the development of future emission scenarios. Not surprisingly for China, which has experienced drastic reductions in emissions due to the enforcement of stringent air quality policies, the trends from the strong pollution control scenarios, SSP1 and SPP5, are most representative of the actual recent trend. In India and Western Africa, regions of rapid population growth and significant increases in unregulated emissions, SSP3 and SSP4 which represent futures with more pessimistic development trends (e.g. little investment in health and education and fast growing populations) match most closely the actual recent trends.

Acknowledgments

This study has received support from the CAMS (Copernicus Atmospheric Monitoring System) project and contributes to the AMIGO (Analysis of eMIssions usinG Observations, https://amigo.aeronomie.be/) project of the International Global Atmospheric Cjemistry (IGAC) project. This research (MB) has also been supported by the projects PRODEX TROVA (2016-2018) and TROVA-E2 (2019) of the European Space Agency (ESA) funded by the Belgian Science Policy Office, as well as by the SOLFEO project funded by ESA. We acknowledge the use of data products from the NASA AURA and EOS Terra satellite missions. We also acknowledge the free use of tropospheric NO2 column data from the SCIAMACHY, GOME-2, and OMI sensors from www.temis.nl. Part of this work was conducted at the Jet Propulsion Laboratory, California Institute of Technology, under contract with the National Aeronautics and Space Administration (NASA).

References

Arellano, A. F., Kasibhatla, P. S., Giglio, L., Van der Werf, G. R., & Randerson, J. T. (2004). Top-down estimates of global CO sources using MOPITT measurements. *Geophys. Res. Lett., 31*, doi:10.1029/2002GL015609.

Bey, I., Jacob, D., Yantosca, R., Logan, J. A., Field, B., Fiore, A., . . . Schultz, M. (2001). Global modeling of tropospheric chemistry with assimilated meteorology: Model description and evaluation. *Journal of Geophysical Research, 106*, 23073-23095. https://doi.org/10.1029/2001JD000807.

Bouwman, A., Kram, T., & Klein Goldewijk (eds), K. (2006). *Integrated modelling of global environmental change. An overview of IMAGE 2.4.* Netherlands Environmental Assessment Agency (MNP) publications.

Cao, H., Fu, T.-M., Zhang, L., Henze, D., Miller, C., Lerot, C., . . . Zhao, Y. (2018). Adjoint inversion of Chinese non-methane volatile organic compound emissions using space-based observations of formaldehyde and glyoxal. *Atmos. Chem. Phys., 18*, 15017–15046, https://doi.org/10.5194/acp-18-15017-2018.

Chen, C., Dubovik, O., Henze, D. K., Chin, M., Lapyonok, T., Schuster, G. L., . . . Torres, B. (2019). Constraining global aerosol emissions using POLDAR/PARASOL satellite remote sensing observations. *Atmos. Chem. Phys.*, 14585-14606, doi:10.5194/acp-19-14585-2019.

Chen, C., Dubovik, O., Henze, D. K., Lapyonak, T., Chin, M., Ducos, F., . . . Li, L. (2018). Retrieval of desert dust and carbonaceous aerosol emissions over Africa from POLDER/PARASOL products generated by the GRASP algorithm. *Atmos. Chem. Phys.*, 12551-12580, doi:10.5194/acp-18-12551-2018.

Crippa, M., Guizzardi, D., Muntean, M., Schaaf, E., Dentener, F., Aardenne, J. A., . . . Janssens-Maenhout, G. (2018). Gridded emissions of air pollutants for the period 1970-2012 with EDGARv4.3.2. *Earth Syst. Sci. Data, 10*, 1987-2013, https://doi.org/10.5194/essd-10-1987-2018.

Ding, J., A, R. v., Mijling, B., & Levelt, P. (2017). Space-based NOx emission estimates over remote regions improved in DECSO. *10*, 925-938.

Dubovik, O., Herman, M., Holdak, A., Lapyonok, T., Tanré, D., Deuzé, J. L., . . . Lopatin, A. (2011). Statically optimized inversion algorithm for enhanced retrieval of aerosol properties from spectral and mutli-angle polarimetric satellite observations. *Atmos. Meas. Tech., 4*, https://doi.org/10.5194/amt-4-975-2011.

Dubovik, O., Lapyonok, T., Litvinov, P., Herman, M., Fuertes, D., Ducos, F., . . . Federspiel, C. (2014). GRASP: a versatile algorithm for characterizing the atmosphere. *SPIE Newsroom*, https://doi.org/10.1117/2.1201408.005558.

Elbern, H., Schmidt, H., & Ebel, A. (1997). Variational data assimilation for tropospheric chemistry modeling. *J. Geophys. Res. Atmos., 102*, doi:10.1029/97JD01213.

Eyring, V., Bony, S., Meehl, G., Senior, C., Stevens, B., Stouffer, R., & Taylor, K. (2016). Overview of the Coupled Model Intercomparison Project Phase 6 (CMIP6) experimental design and organization. *Geoscientific Model Development, 9*, https://doi.org/10.5194/gmd-9-1937-1026.

Gidden, M. J., Riahi, K., Smith, S. J., Fujimori, S., Luderer, G., Kriegler, E., . . . Fricko, O. (2019). Global emissions pathways under different socioeconomic scenariosfor use in CMIP6: a dataset of harmonized emissions trajectoriesthrough the end of the century. *Geosci. Model Dev.,*, 1443–1475, https://doi.org/10.5194/gmd-12-1443-2019.

Granier, C., Bessagnet, B., Bond, T., & al., e. (2011). Evolution of anthropogenic and biomass burning emissions of air pollutants at global and regional scales during the 1980-2010 period. *Climate Change, 109*, https///doi.org/10.1007/s10584-011-0154-1.

Granier, C., Darras, S., Gon, H. D., Doubalova, J., Elguindi, N., Galle, B., . . . Sindelarova, K. (2019). *The Copernicus Atmosphere Monitoring Service global and regional emissions.* Copernicus Atmosphere Monitoring Service.

He, T.-L., Jones, D. B., Huang, B., Liu, Y., Miyazaki, K., Jiang, Z., . . . Worden, J. R. (2019). Recurrent U-net: Deep learning to predict daily summertime ozone in the United States. arXiv:1908.05841.

Henze, D. K. (2009). Inverse modeling and mapping US air quality influences of inorganic PM2.5 precursor emissions using the adjoint of GEOS-Chem. *Atmos. Chem. Phys., 9*, 5877-5903.

Henze, D. K., Hakami, A., & Seinfeld, J. H. (2007). Development of the adjoint of GEOS-Chem. *Atmos. Chem. Phys., 7*, doi:10.5194/acp-7-2413-2007.

Hosley, R., Smith, S., Feng, L., Klimont, Z., Janssens-Maenhout, G., Pitkanen, T., . . . al., e. (2018). Historical (1750-2014) anthropogenic emissions of reactive gases and aerosols from the Community Emissions Data System (CEDS). *Geosci. Model Dev., 11*, http://doi.org/10.5194/gmd-11-369-2018.

HTAPv2. (???). HTAPv2. www.htap.org.

Jiang, Z. D. (2011). Quantifying the impact of modelerrors on top-down estimates of carbon monoxide emissions using satellite observations. *J. Geophys. Res., 116*, D15306,doi:10.1029/2010JD015282.

Jiang, Z., Jones, D., Worden, H., Deeter, M., Henze, D., Worden, J., . . . Schuck, T. (2013). Impact of model errors in convective transport on CO source estimates inferred from MOPITT CO retrievals. *J. Geophys. Res. Atmos., 118*, doi:101002/jgrd.50216.

Jiang, Z., Jones, D., Worden, J., Worden, H., Henze, D., & Wang, Y. (2015). Regional data assimilation of multi-spectral MOPITT observations of CO over North America. *Atmos. Chem. Phys.*, 6801-6814, doi:10.5194/acp-15-6801-2015.

Jiang, Z., Worden, J., Worden, H., M. Deeter, D. J., Arellano, A., & Henze, D. (2017). A 15-year record of CO emissions constrained by MOPITT CO observations. *Atmos. Chem. Phys., 17*, 4565-4583.

Keita. (2020). DACCIWA. *Journal of ???*

Kriegler, E., Edmonds, J., Hallegatte, S., K.L., E., Kram, T., Riahi, K., . . . Vuuren, D. v. (2014). A new scenario framework for climate change research: the concept of shared climate policy assumptions. *122*, 401-414.

Krotkov, N. A., Lamsal, L. N., Celarier, E., Swartz, W., Marchenko, S., Bucsela, E. J., & al, e. (2017). The version 3 OMI NO2 standard product. *Atmospheric Measurement Techniques, 10*, https://doi.org/10.5194/amt-10-3133-2017.

Kuenen, J., Visschedijk, A. J., Jozwicka, M., & Denier van der Gon, H. (2014). TNO-MACC_II emission inventory: a multi-year (2003–2009) consistent high-resolution European emission inventory for air quality modelling. *Atmos. Chem. Phys*, 10963-10976, doi:10.5194/acp-14-10963-2014.

Kurokawa, J., & Ohara, T. (2019). Long-term historical trends in air pollutant emissions in Asia: Regional Emission inventory in ASia (REAS) version 3.1. *Atmos. Chem. Phys. Discuss.*, https://doi.org/10.5194/acp-2019-1122.

Laughner, J., & Cohen, R. (2019). Direct observation of changing NOx lifetime in North American cities. *Science, 366*, 723-727, doi: 10.1126/science.aax6832.

Li, C., Joiner, J., Krotkov, N. A., & Bhartia, P. (2013). A fast and sensitive new satellite SO2 retrieval algorithm based on principal component analysis: Application to the Ozone Monitoring Instrument. *Geophysical Research Letters, 40*, https://doi.org/10.1002/2013GL058134.

Li, J., & Y.Wang. (2019). Inferring the anthropogenic NOx emission trend over the United States during 2003-2017 from satellite observations: Was there a flattening of the emission trend after the Great Recession? *Atmos. Chem. Phys. Disc.*, https://doi.org/10.5194/acp-2019-472.

Li, M. Z. (2019). Persistent growth of anthropogenic non-methane volatile organic compound (NMVOC) emissions in China during 1990–2017: drivers, speciation and ozone formation potential. *Atmos. Chem. Phys., 19*, 8897–8913, https://doi.org/10.5194/acp-19-8897-2019.

Li, M., Zhang, Q., Streets, D. G., He, K. B., Cheng, Y. F., Emmons, L. K., . . . Zhang, Y. (2014). Mapping Asian anthropogenic emissions of non-methane volatile organic compounds to multiple chemical mechanisms. *Atmos. Chem. Phys., 14*, 5617-2014.

Liousse, C., Assamoi, E., Criqui, P., Granier, C., & Rosset, R. (2014). Explosive Growth in African combustion emissions from 2005 to 2030. *Environmental Research Letters, 9*, doi:10.1088/1748-9326/9/3/035003.

Liu, F. Z., Li, M., Huo, H., & He, K. B. (n.d.).

Liu, F., Zhang, Q., Tong, D., Zheng, B., Li, M., Huo, H., & He, K. B. (2015). High-resolution inventory of technologies, activities, and emissions of coal-fired power plants in China from 1990 to 2010. *Atmos. Chem. Phys., 15*, doi:10.5194/acp-15-13299-2015.

Müller, J.-F. T.-F. (2018). Top-Down CO Emissions Based on IASI Observations and Hemispheric Constraints on OH Levels. *Geophysical Research Letters, 45*, http://doi.org/10.1002/2017GL076697.

Müller, J.-F., & Stavrakou, T. (2005). Inversion of CO and NOx emissions using the adjoint of the IMAGES model. *Atmos. Chem. Phys., 5*, https://doi.org/10.5194/acp-5-1157-2005.

MACCity. (n.d.). MACCity. https://eccad3.sedoo.fr.

Marais, E., & Wiedinmyer, C. (2016). Air Quality Impact of Diffuse and Inefficient Combustion Emissions in Africa (DICE-Africa). *Environmental Science and Technology, 50*, doi:10.1021/acs.est.6b02602.

Martin, R. V., Jacob, D. J., Chance, K., Kurosu, T. P., Palmer, P. I., & Evans, M. J. (2003). Global inventory of nitrogen oxide emissions constrained by space-based observations of NO2 columns. *J. Geophys. Res. Atmos., 108*, doi:10.1029/2003JD003453.

MEICv1.3. (n.d.). MEICv1.3. http://www.meicmodel.org.

Menut, L., Bessagnet, B., Khovorostyanov, D., Beekman, M., Blond, N., Colette, A., . . . Vivanco, M. (2013). CHIMERE 2013: a model for regional atmospheric composition modelling. *Geosci. Model Dev., 6*, doi:10.5194/gmd-6981-2013.

Mijling, B., & A, A. v. (2012). Using daily satellite observations to estimate emissions of short-lived air pollutants on a mesoscopic scale. *J. Geophys. Res. Atmos., 117*, doi:10.1029/2012JD017817.

Miyazaki, K. B. (2020). Evaluation of a multi-model, multi-constituent assimilation framework for tropospheric chemical reanalysis. *Atmos. Chem. Phys. Discuss.*, https://doi.org/10.5194/acp-2019-645, in press.

Miyazaki, K., Bowman, K., Sekiya, T., Eskes, H., Boersma, F., Worden, H., . . . Ogochi, K. (2020). An updated tropospheric chemistry reanalysis and emission estimates, TCR-2, for 2005-2018. *Earth Syst. Sci. Data Discuss.*, submitted.

Miyazaki, K., Eskes, H., Sudo, K., Boersma, K. F., Bowman, K., & Kanaya, Y. (2017). Decadal changes in global surface NOx emissions from multi-constituent satellite data assimilation. *Atmos. Chem. Phys., 17*, doi:10.5194/acp-17-807-2017.

Miyazaki, K., Eskes, H., Sudo, K., Boersma, K. F., Bowman, K., & Kanaya, Y. (2019). Balance of emission and dynamical controls on ozone during the Korea¿United States Air Quality campaign from multiconstituent satellite data assimilation. *Journal of Geophysical Research: Atmospheres, 124*, 387-413.

NEI. (2018). National Emission Inventory for the U.S. https://www.epa.gov/air-emissions-inventories/.

O'Neill, B., Tebaldi, C., Vuuren, D. v., Eyring, V., Friedlingstein, P., Hurtt, G., . . . Sanderson, B. M. (2016). The Scenario Model Intercomparison Project (ScenarioMip) for CMIP6. *GeoSci. Model Dev., 9*, doi:10.5194/gmd-9-3461-2016.

Qu, Z., Henze, D. K., Capps, S. L., Wang, Y., Xu, X., Wang, J., & Keller, M. (2017). Monthly top-down NOx emissions for China (2005¿2012): A hybrid inversion method and trend analysis. *J. Geophys. Res. Atmos., 122*, 4600-4625.

Qu, Z., Henze, D. K., Li, C., Theys, N., Wang, Y., Wang, J., . . . Ren, X. (2019). SO2 Emission Estimates Using OMI SO2 Retrievals for 2005-2017. *J. Geophys. Res. Atmos., 124*, https://doi.org/10.1029/2019JD030243.

Qu, Z., Henze, D. K., Theys, N., Wang, J., & Wang, W. (2019). Hybrid Mass Balance/4D-Var Joint Inversion of NOx and SO2 Emissions in East Asia. *J. Geophys. Res. Atmos., 124*, doi:10.1029/2018JD030240.

Rao, S., Klimont, Z., J.Smith, S., Dingenen, R. V., Dentener, F., Bouwman, L., . . . Calvin, K. (2016). Future air pollution in the Shared Socio-economic Pathways. *Global Environmental Change*, https://doi.org/10.1016/j.gloenvcha.2016.05.012.

Riahi, K., Vureen, D. v., & Kriegler, E. (2017). The Shared Socioeconomic Pathways and their energy, landuse, and greenhouse gas emissions implications : An overview. *Global Environmental Change, 42*, 153-168.

Stavrakou, T., Müller, J.-F., Bauwens, M., Smedt, I. D., Roozendael, M. V., Mazière, M. D., . . . Guenther, A. (2015). How consistent are top-down hydrocarbon emissions based on formaldehyde observations from GOME2 and OMI? *Atmos. Chem. Phys., 15*, 11861-11884.

Stavrakou, T., Müller, J.-F., Boersma, K. F., van der A, R. J., Kurokawa, J., Ohara, T., & Zhang, Q. (2013). Key chemical NOx sink uncertainties and how they influence top-down emissions of nitrogen oxides. *Atmos. Chem. Phys., 13*, 9057-9082, https://doi.org/10.5194/acp-13-9057-2013.

Stavrakou, T., Müller, J.-F., De Smedt, I., Van Roozendael, M., van der Werf, G. R., Giglio, L., & Guenther, A. (2009). Evaluating the performance of pyrogenic and biogenic emission inventories against one decade of space-based formaldehyde columns. *Atmos. Chem. Phys., 9*, https://doi.org/10.5194/acp-9-1037-2009, 2009.

Stavrakou, T., Müller, J.-F., Peeters, J., Razavi, A., Clarisse, L., Clerbaux, C., . . . Paton-Walsh, C. (2012). Satellite evidence for a large source of formic acid from boreal and tropical forests. *Nature Geosci., 5*, https://doi.org/10.1038/ngeo1354.

Sun, W., Shao, M., Granier, C., Liu, Y., Ye, C., & Zheng, J. (2018). Long-term trends of Anthropogenic SO2, NOx, CO, and NMVOCs Emissions in China. *Earth's Future, 6*, 1112-1133, https://doi.org/10.1029/2018EF000822.

Theys, N., Smedt, I. d., Gent, J. v., Danckaert, T., Wang, T., Hendrick, F., & al., e. (2015). Sulfur dioxide vertical column DOAS retrievals from the Ozone Monitoring Instrument: Global observations and comparison to ground-based and satellite data. *Journal of Geophysical Research: Atmospheres, 120*, https://doi.org/10.1002/2014JD022657.

van Vuuren, D., Edmonds, J., Kainuma, M., & al., e. (2011). The representative concentration pathways: an overview. *Climate Change, 109*, https://doi.org/10.107/s10584-011-0148-Z.

Watanabe, S., Hajima, T., Sudo, K., Nagashima, T., Takemura, T., Okajima, H., . . . Kawamiya, M. (2011). MIROC-ESM 2010: model description and basic results ofCMIP5-20c3m experiments. *Geosci. Model Dev.*, 845–872, doi:10.5194/gmd-4-845-2011.

Zhang, Q., Streets, D. G., Carmichael, G. R., He, K. B., Huo, H., Kannari, A., . . . Yao, Z. L. (2009). Asian emissions in 2006 for the NASA INTEX-B mission. *Atmos. Chem. Phys., 9*, 5131-5153.

Zheng, B., Chevallier, F., Ciais, P., Yin, Y., & Wang, Y. (2018). On the role of the flaming to smoldering transition in the seasonal cycle of African fire emissions. *Geophys. Res. Lett., 45*, doi: 10.1029/2018GL079092.

Zheng, B., Chevallier, F., Ciais, P., Yin, Y., Deeter, M., Worden, H., . . . He, K. B. (2018). Rapid decline in carbon monoxide emissions and export from East Asia between years 2005 and 2016. *Environ. Res. Lett., 13*, doi: 10.1088/1748-9326/aab2b3.

Zheng, B., Chevallier, F., Yin, Y., Ciais, P., Fortems-Cheiney, A., Deeter, M. N., . . . Zhao, Y. (2019). Global atmospheric carbon monoxide budget 2000¿2017 inferred from multi-species atmospheric inversions. *Earth Syst. Sci. Data, 11*, doi:10.5194/essd-2019-61.

Zheng, B., Huo, H., Zhang, Q., Yao, Z. L., Wang, X. T., Yang, X. F., . . . He, K. B. (2014). High-resolution mapping of vehicle emissions in China in 2008. *Atmos. Chem. Phys., 14*, doi:10.5194/acp-14-9787-2014.

Zheng, B., Tong, D., Li, M., Liu, F., Hong, C., Geng, G., . . . Zhang, Q. (2018). Trends in China's anthropogenic emissions since 2010 as the consequence of clean air actions. *Atmos. Chem. Phys., 18*, doi:10.5194/acp-18-14095-2018.

Zhu, L. M., Sheng, J., Hu, L., Gonzalez Abad, G., & Chance, K. (n.d.).

Zhu, L., Jacob, D. J., Kim, P. S., Fisher, J. A., Yu, K., Travis, K. R., . . . Wolfe, G. M. (2016). Observing atmospheric formaldehyde (HCHO) from space: validation and intercomparison of six retrievals from four satellites (OMI, GOME2A, GOME2B, OMPS) with SEAC4RS aircraft observations over the southeast US. *Atmos. Chem. Phys., 16*, https://doi.org/10.5194/acp-16-13477-2016.

Zhu, L., Mickley, L. J., Jacob, D. J., Marais, E. A., Sheng, J., Hu, L., . . . Chance, K. (2017). Long-term (2005-2014) trends in formaldehyde columns across North America as seen by the OMI satellite instrument; Evidence of changing emissions of volatile organic compounds. *J. Geophys. Res., 44*, 7079-7086.